Location-Based Multi-site Coordination Beam Tracking for Vehicle mmWave Communications

Xingwen He(✉), Danpu Liu, and Zhilong Zhang

Beijing Laboratory of Advanced Information Networks, Beijing Key Laboratory of Network System Architecture and Convergence, Beijing University of Posts and Telecommunications, Beijing 100876, People's Republic of China
{hexingwen, dpliu, zhangzhilong}@bupt.edu.cn

Abstract. Millimeter wave (mmWave) system with massive multiple input multiple output (mMIMO) meets increasing data traffic requirements. However, fast beam tracking for vehicles with high mobility causes enormous overhead, especially in an ultra-dense network (UDN) with frequently base station (BS) handover. In this paper, we proposed a multi-site coordination beam tracking scheme utilizing the spatial correlation of channel state information (CSI) among different sites to reduce the signaling overhead for beam training and handover. The scenario is a hyper-cellular network (HCN) with one control-BS (CBS) and multiple traffic-BSs (TBSs). The proposed scheme consists of two stages. In the first stage, more accurate position measurement of the moving user equipment (UE) can be achieved by using uniform planar array (UPA), and Extended Kalman Filter (EKF) is exploited in CBS to predict the UE's location in the next slot. In the second stage, the relationship between multi-site and UE's location is used by the CBS to remotely infer the candidate beam between each TBS and the UE, and make a TBS handover decision when necessary. Given that it is the CBS in charge of beam tracking between all the TBSs and the UE centrally, the overhead for beam training and handover are both efficiently reduced. Simulation results based on realistic 3D scenario show that the proposed scheme can achieve 99% of the optimal spectral efficiency with fewer overhead for beam sweeping and handover signaling.

Keywords: Beam tracking · Vehicle network · Multi-site · Extended Kalman filter · Uniform planar array · Handover

1 Introduction

In recent years, the fifth generation (5G) mobile communications developed rapidly. As a typical scenario in 5G, vehicle environment has received widespread attention. Advanced technologies such as high precise road map, real-time position updating and autonomous driving enhance the convenience and safety of driving. However, those applications heavily rely on the vehicle network's support for high capacity and low latency in data sharing.

H. Gao et al. (Eds.): ChinaCom 2020, LNICST 352, pp. 271–287, 2021.
https://doi.org/10.1007/978-3-030-67720-6_19

The mmWave candidates to improve network capacity and increase data rate in 5G, thanks to its huge spectral bandwidth at high frequencies from 30 GHz to 300 GHz. Meanwhile, massive multiple input multiple output (mMIMO) is used to overcome high propagation path loss of mmWave channels [1]. Power is concentrated into one or more beams to communicate with remote users through beamforming. However, the cost of obtaining higher beamforming gain is that the beam gets narrower. Vehicles with high mobility may leave the coverage of one beam easily, resulting in frequent beam misalignment. A traditional approach to address this issue is to periodically transmit training beams to different directions sequentially in time and choose the direction with the largest received signal-to-noise ratio (SNR) [2]. However, the signaling overhead for simple beam sweeping is not acceptable in high mobility scenario, hence more fast and efficient beam tracking methods are needed.

Some prior work of beam tracking considers to utilize the temporal correlation between channel to improve the efficiency of beam alignment. On one hand, authors in [3] define a novel concept called beam coherence time which is an effective measure of beam alignment frequency. On the other hand, Kalman Filter plays an important role in positioning and beam tracking to reduce pilot overhead and required SNR. In [4], a linear Kalman Filter based angle domain channel tracking algorithm was designed to acquire channel state information (CSI) in each coherence time. In [5], authors proposed a Kalman Filter based tracking algorithm which focused on abrupt channel changes (e.g., blockage), slow variations of angles of departure (AoD), and angles of arrival (AoA). [6] proposed an Extended Kalman Filter (EKF)-based algorithm using the position, velocity, and channel coefficient as state variables. Authors in [7] utilized EKF to position prediction and related location-based beamforming for high-speed train (HST) scenario in 5G New Radio (NR) networks. However, most of the above mentioned methods focus on antenna system with uniform linear array (ULA), which resulted in beam alignment errors in real three-dimensional (3D) environment.

Furthermore, in order to meet the rapidly growing demand for mobile data services, ultra-dense network (UDN) reduces the transmission distance between BSs and UE which yields to less path loss and higher traffic density by increasing the number of small BSs [8]. However, there are two major challenge in UDN with high-speed vehicle. 1) A huge number of densely small BSs increase pilot overhead and time for beam alignment. 2) Handover between BSs causes large signaling overhead of core network.

An effective framework in UDN called hyper-cellular network (HCN) is proposed in [9] with separated coverage area of control channel and data channel, where control-BS (CBS) and traffic-BS (TBS) take care of control information and data transmission respectively. In this architecture, CBS performs centralized management and controls TBS selection, which improves system energy efficiency and reduces core network signaling caused by frequent TBS handover in vehicle environment. Because of the common scatters and location-based light-of-sight (LoS) components, the CSIs between geographically separated CBS and TBS emerge nonlinear relevance, which has a great effect on CBS centralized management and scheduling [10]. On this basis, the non-linear correlation between the CSI of TBSs was studied and a neural network-based remote channel interference scheme was proposed to reduce channel acquisition overhead in [11]. Authors in [12] proposed a time-sequence channel learning

framework to predict the beam direction of target roadside unit (RSU) in future steps from the CSI of source RSU in the past period of time.

In this paper, we propose a multi-site coordinated beam tracking method in HCN for vehicle environment to reduce the overhead for beam training and TBS handover. The basic idea is to track the beam direction of TBS based on the UE's position information from CBS, and determine TBS handover from serving TBS to target TBS in each slot. The main challenge is that the precision of position prediction based on beam training has a significant effect on the multi-site coordination performance when UE moves with high velocity in practical three-dimensional mMIMO environment. Hence, we adopt an EKF-based position prediction scheme to improve the estimation accuracy. Besides, UPA with flexible 3D beam direction provides more exact position measurement.

The main contributions of this work are summarized as follows.

1) An efficient EKF based positioning and beam tracking method for wideband 5G systems is proposed, and the associated position measurement based on UPA is also developed.
2) Based on the spatial correlation of multi sites, a geometry based beam inference method is applied to reduce the overhead for beam training. Besides, a novel TBS handover scheme is proposed which jointly considered position and reference signal receiving power (RSRP).
3) The performance of the proposed scheme is evaluated based on ray-tracing channel data in real urban scenario, and the simulation result shows that the spectral efficiency for TBS reaches 99% of the upper bound with lower overhead in beam sweeping and TBS handover.

The rest of paper is organized as follows. Section 2 describes the considered system model, including HCN scenario, channel models and transmit and receive signal structure. In Sect. 3, the proposed location-based multi-site coordination beam tracking scheme is developed and presented. Finally, the performance of the proposed approach is evaluated and analyzed in Sect. 4, while the conclusions are drawn in Sect. 5.

Notation: Bold upper and lower case letters represent matrices and vectors, respectively. The transpose and conjugate transpose of a matrix are denoted as $(\cdot)^T$ and $(\cdot)^H$, respectively. Furthermore, $|\cdot|$ and $\|\cdot\|_2$ represent the modulus of a complex number and the 2-norm of a matrix, respectively.

2 System Model

As shown in Fig. 1, we consider an HCN with one CBS and multiple TBSs, and UE moves straightly along the road with high velocity. In order to save overhead for beam training and TBS handover, the CBS predicts the UE's position in future slots based on EKF, and centrally selects candidate beams for each TBS to communicate with the UE based on geometric method. If the link between the serving TBS and the UE satisfies the condition for handover, the CBS controls TBS handover and sends the predicted

beam direction to TBS through backhaul link. An efficient TBS handover scheme based on UE's location is also proposed.

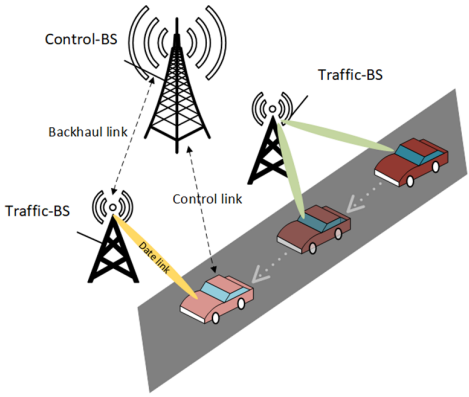

Fig. 1. Schematic of the proposed location-based multi-site coordination beam tracking scheme

Assume that both BSs and the UE are equipped with UPA and single radio frequency (RF) chain. The number of antennas of the BS and UE is $M_{h,BS}$ and $M_{h,UE}$ in each row, $M_{v,BS}$ and $M_{v,UE}$ in each column, respectively. To improve positioning accuracy, a 3D beam steering codebook is adopted to generate the communication beam pairs, which is the Kronecker product of two 2D codebook in vertical and horizontal direction, i.e.

$$\mathbf{F}_{RF}=\mathbf{F}_{RF,v} \otimes \mathbf{F}_{RF,h} \tag{1}$$

where

$$\mathbf{F}_{RF,v}(m,k) = \frac{1}{\sqrt{M_{v,UE}}} \exp\left(j\frac{2\pi}{\lambda} d_v m \sin\left(\frac{2\pi k}{2^K}\right)\right) \tag{2}$$

$$\mathbf{F}_{RF,h}(m,k) = \frac{1}{\sqrt{M_{h,UE}}} \exp\left(j\frac{2\pi}{\lambda} d_h m \sin\left(\frac{2\pi k}{2^K}\right)\right) \tag{3}$$

where λ is the wavelength of carrier frequency, d_v and d_h denotes the distance between adjacent antennas in vertical and horizontal, respectively, which are equal to the half of wavelength. K denotes quantization resolution of AoA/AoD.

For the uplink, an analog precoder $\mathbf{f}_{RF} \in \mathbb{C}^{M_{v,UE}M_{h,UE}\times 1}$ is applied at UE, and single data stream is precoded and then transmitted on each antenna. As $\mathbf{f}_{RF}$ is implemented with the phase shifter which can only change the phase of transmitted signal, each element of $\mathbf{f}_{RF}$ has a unitary magnitude, i.e. $|\mathbf{f}_{RF}(i,j)| = \frac{1}{\sqrt{M_{v,UE}M_{h,UE}}}$. At the BS, the received signals are firstly processed by an analog combiner $\mathbf{w}_{RF} \in \mathbb{C}^{M_{v,BS}M_{h,BS}\times 1}$, which is generated by the phase shifter similar with $\mathbf{f}_{RF}$ that $|\mathbf{w}_{RF}(i,j)| = \frac{1}{\sqrt{M_{v,BS}M_{h,BS}}}$.

The detected signal at BS can be written as

$$\mathbf{r}_t = \mathbf{w}_{RF}^H \mathbf{H}_t \mathbf{f}_{RF} \mathbf{s}_t + \mathbf{w}_{RF}^H \mathbf{n} \tag{4}$$

where, $\mathbf{s}_t \in \mathbb{C}^{1\times N_s}$ which consists of N_s sampling points is the uplink orthogonal frequency-division multiplexing (OFDM) signal at time t, and can be written as $\mathbf{s}_t = [\mathbf{s}_t(0), \mathbf{s}_t(1), \ldots, \mathbf{s}_t(N_s)]$, where the n-th sampling point is defined as

$$\mathbf{s}_t(n) = \frac{1}{N}\sum_{k=0}^{N-1} S(k) e^{j\frac{2\pi}{N}kn} \tag{5}$$

where, $S(k)$ is the k-th subcarrier of OFDM symbol, and N denotes the number of subcarriers. $\mathbf{n} \in \mathbb{C}^{M_{v,BS}M_{h,BS}\times N_s}$ denotes the additive white Gaussian noise, each entry of which follows the independent and identically distributed (i.i.d.) complex Gaussian distribution with zero mean and variance σ_n^2.

Furthermore, according to the multi-path time-varying channel model in [13], the uplink channel vector is given by

$$\mathbf{H}_t = \sum_{l=0}^{L-1} \alpha_{l,t} e^{-j\left(\phi_{l,t}+\phi_{f_d,l,t}\right)} \mathbf{a}\left(\theta_{l,t}^{tx}, \varphi_{l,t}^{tx}\right) \mathbf{a}^T\left(\theta_{l,t}^{rx}, \varphi_{l,t}^{rx}\right) \delta\left(t-\tau_{l,t}\right) \tag{6}$$

where, $l = 0$ corresponds LoS path, and other parameters are discussed in detail below. $\alpha_{l,t}$ denotes complex gain based on path loss and shadowing, $\tau_{l,t} = d_{l,t}/c$ denotes corresponding delay for the l-th path whose length is $d_{l,t}$. $\theta_{l,t}^{tx}, \theta_{l,t}^{rx} \in [-\pi, \quad \pi)$ and $\varphi_{l,t}^{tx}, \varphi_{l,t}^{rx} \in [0, \quad \pi)$ denote the azimuth and elevation angle of the l-th path of UE and BS, respectively. $\phi_{l,t}=2\pi f_c \tau_{l,t}$ denotes the phase caused by carrier frequency f_c, $\phi_{f_d,l,t}=2\pi f_{d,l,t} t$ denotes Doppler phase shift for the l-th path. The Doppler shift for the l-th path is defined as $f_{d,l,t}=\frac{v\cos\theta_{l,t}^{tx}\cos\varphi_{l,t}^{tx}}{\lambda}$, where v is the velocity of UE. $\mathbf{a}\left(\theta_{l,t}^{tx}, \varphi_{l,t}^{tx}\right)$ and $\mathbf{a}\left(\theta_{l,t}^{rx}, \varphi_{l,t}^{rx}\right)$ denotes the UPA steering vector of the UE and the BS respectively. We assume that the UPA is deployed on y-z plane. By taking the UE side as example, the steering vector can be written as

$$\mathbf{a}\left(\theta_{l,t}^{tx}, \varphi_{l,t}^{tx}\right) = \mathbf{a}_v\left(\theta_{l,t}^{tx}, \varphi_{l,t}^{tx}\right) \otimes \mathbf{a}_h\left(\theta_{l,t}^{tx}, \varphi_{l,t}^{tx}\right) \tag{7}$$

where $\otimes$ denotes the Kronecker product, and the steering vector in vertical and horizontal are written as

$$\mathrm{a}_v\left(\theta_{l,t}^{tx}, \varphi_{l,t}^{tx}\right) = \frac{1}{\sqrt{M_{v,BS}}}\left[1, e^{j\frac{2\pi}{\lambda}d_v \sin\theta_{l,t}^{tx}}, \ldots, e^{j\left(M_{v,BS}-1\right)\frac{2\pi}{\lambda}d_v \sin\theta_{l,t}^{tx}}\right]^T \tag{8}$$

$$\mathrm{a}_h\left(\theta_{l,t}^{tx}, \varphi_{l,t}^{tx}\right) = \frac{1}{\sqrt{M_{h,BS}}}\left[1, e^{j\frac{2\pi}{\lambda}d_h \cos\theta_{l,t}^{tx} \sin\varphi_{l,t}^{tx}}, \ldots, e^{j\left(M_{h,BS}-1\right)\frac{2\pi}{\lambda}d_h \cos\theta_{l,t}^{tx} \sin\varphi_{l,t}^{tx}}\right] \tag{9}$$

When data is transmitted from the TBS to the UE, the spectral efficiency can be expressed as

$$R_s = \log_2\left(1 + \frac{P_{TBS}}{\sigma_n^2}\frac{\mathbf{w}_{RF}^H \mathbf{H}\mathbf{f}_{RF}\mathbf{f}_{RF}^H \mathbf{H}^H \mathbf{w}_{RF}}{\mathbf{w}_{RF}^H \mathbf{w}_{RF}}\right) \tag{10}$$

where P_{TBS} is the power of TBS transmitted signal.

3 Location-Based Multi-site Coordination Beam Tracking

In this section, we propose a location-based multi-site coordination beam tracking scheme in HCN for vehicle environment. In spite of mMIMO system with beamforming enhances the spectral efficiency by concentrating signal power on one or more beams, beam misalignment caused by high mobility in vehicle environment leads to frequently beam sweeping, thus increases overhead of beam training. In the proposed framework, we focus on finding the optimal beam of the TBS based on coordinated position prediction by the CBS with low beam training overhead.

In order to introduce the proposed method, we first give some high-level analysis. The optimal beam pattern of TBS is determined by the CSI at TBS, and it can be obtained by the CSI of CBS as well as the spatial correlation of CSI between the CBS and the TBS. However, due to the high complexity of calculating the full-dimensional CSI estimation in mMIMO, we transform the beam inferred problem into angle domain. Note that the correlation of angle domain CSI is mainly decided by the AoA from the UE to the CBS and the TBS. Moreover, the beam direction is strongly connected with the AoA of LoS. Therefore, the optimal beam pattern of each TBS can be inferred by the UE's position. Besides, considering the temporal correlation of channel, we can predict the UE's position in each time step by EKF, so that the positioning accuracy is improved.

Therefore, the proposed method is divided into two stages, i.e. position prediction stage and multi-site coordination stage. In position prediction stage, the CBS estimates the time of arrival (ToA) and AoA of the UE from the received uplink pilot to obtain the UE's position. At the same time, based on the estimated position and the temporal correlation of positions in motion function, the EKF is used to predict the UE's position in the future. In multi-site coordination stage, the CBS determines TBSs' candidate beams for downlink data transmission on the basis of the geometric relationship between the predicted UE's position and multiple TBSs' position. Subsequently, the CBS controls TBS handover based on position and RSRP jointly. As a result, the beam searching complexity and overhead for handover signaling are both reduced.

3.1 EKF-Based Position Prediction

In this part, we propose an EKF-based position prediction scheme. The EKF obtains a more accurate state estimation, according to combining the initial state estimation of the system at the next moment, and the feedback obtained from the measurement. That is why the EKF is an effective method in trajectory prediction problems with nonlinear model function.

In order to reduce measurement error and enhance estimation performance of EKF in the proposed scheme, UPA is equipped on both BSs and UE to provide more accurate spatial position information in 3D mMIMO scenario. In this part, position measurement based on the received signal of UPA is introduced first, then the EKF procedure used for position prediction is presented.

Position Measurement

Consider a UE located at any point P with coordinates (p_x, p_y, p_z) in Space rectangular coordinate system, and the CBS located at the origin. A major concern is that the CBS has difficulty measuring the UE's coordination directly. However, directional beam between the CBS and the UE will provide angle domain information. Consequently, we indicate the UE's location in spherical coordinate (R, θ, φ), where R denotes the distance between the CBS and the UE, θ and φ denotes azimuth and elevation AoA of LoS. The distance is expressed as the product of TOA for LoS path and the speed of light. Therefore, the position measurement is based on TOA and AoA estimation for LoS.

The estimation of ToA and AoA is based on the periodic UL SRS transmitted by the UE, however, the major problem is the multi-path effect. The transmitted signal arrives at receiver side through multi-path with different propagation delays and angles, which causes delay spread and angle spread for received signal. Instead of extracting channel parameters with complex calculation, correlation analysis and beam sweeping are utilized for TOA and AoA estimation.

We assume that the control link between the CBS and the UE is unblocked, the LoS component in the received signal has the maximum power, thus the LoS component in received signal has the strongest correlation with the transmitted signal. Hence, the TOA of LoS can be estimated by cross-correlation between the received signal and the known SRS, and the correlation method takes advantages of processing low SNR signals.

The cross-correlation function observed in the CBS can be written as

$$\mathbf{c}[n] = \sum_{m=0}^{N_s-1} \mathbf{s}^*(n-m)\mathbf{r}(m) \tag{11}$$

where $\mathbf{s}(m)$ is the known SRS transmitted from UE. We neglect the synchronized error between CBS and UE. By finding the sample index where the absolute value of correlation is maximum, the estimation of TOA can be obtained, and is written as $\hat{\tau} = \frac{\hat{n}}{F_s}$, where $\hat{n} = \arg\max_n |\mathbf{c}[n]|$ denotes the estimated TOA in samples and F_s is the sampling frequency.

After the ToA has been estimated, we will execute AoA estimation by beam sweeping. Due to multipath with different AoAs, the received signal consists of LoS and NLoS components, i.e. $\mathbf{y}_{los}$ and $\mathbf{y}_{nlos}$. Beamforming is used to compensate the phase difference of $\mathbf{y}_{los}$ by controlling the phase shifter, so that the amplitude of $\mathbf{y}_{los}$ from different antennas increases after combining. On the contrary, $\mathbf{y}_{nlos}$ will not obtain beamforming gain due to the phase delay of the phase shifter does not match the phase difference of $\mathbf{y}_{nlos}$ on each antenna.

According to the previous analysis, the beam direction with the highest received power can be regarded as the direction of LoS based on the above assumption that LoS exists. The specific process is shown as follows.

Firstly, the CBS chooses the optimal received beam by maximizing received signal power. The corresponding codeword is defined as

$$\hat{\mathbf{w}}_{i_q} = \arg\max_{\mathbf{w}_{i_q}} \left\{ \left(\left\| \mathbf{w}_{i_q}^H y \right\|_2 \right)^2 \right\} \tag{12}$$

where i_q is the candidate beam index. The set of candidate beam index is given as $I = \{i_q | q = 1, \ldots, Q\}$, where Q is the size of candidate beams. In initialization stage, the CBS performs exhaustive beam sweeping to connect with the UE, which means Q equals to the total number of CBS beams. Once the UE's position is predicted, the CBS performs narrow-range beam sweeping around the estimated AOA in last time step, and Q can be set in a small value.

After the best received beam is identified through beam sweeping, we need to determine the azimuth and elevation AOA, i.e. θ and φ, according to the corresponding codeword $\hat{\mathbf{w}}_{i_q}$. We assumed that the number of antenna and the distance between adjacent antennas in horizon and vertical are equal to M and d, respectively. According to the analysis above, $\hat{\mathbf{w}}_{i_q}$ can be expressed as the conjugate transpose of the steering vector, and is written as

$$\hat{\mathbf{w}}_{i_q} = \frac{1}{M} \left[1, \ldots, e^{-j\frac{2\pi}{\lambda} d(m_v \sin\theta + m_h \cos\theta \sin\varphi)}, \ldots, e^{-j(M-1)\frac{2\pi}{\lambda} d(\sin\theta + \cos\theta \sin\varphi)} \right]^T \tag{13}$$

Furthermore, $\hat{\mathbf{w}}_{i_q}$ can be represented as the Kronecker product of $\hat{\mathbf{w}}_{i_q,h}$ and $\hat{\mathbf{w}}_{i_q,v}$, where $\hat{\mathbf{w}}_{i_q,h} \in \mathbb{C}^{M\times 1}$ and $\hat{\mathbf{w}}_{i_q,v} \in \mathbb{C}^{M\times 1}$ are the codeword in horizon and vertical directions, respectively. Therefore, θ and φ can be estimated by the main lobe angle of $\hat{\mathbf{w}}_{i_q,v}$ and $\hat{\mathbf{w}}_{i_q,h}$, i.e. $\hat{\alpha}_{i_q,v}$ and $\hat{\alpha}_{i_q,h}$.

Finally, based on (13), the azimuth and elevation AOA can be estimated by

$$\hat{\theta} = \hat{\alpha}_{i_q,v} \tag{14}$$

$$\hat{\varphi} = \arcsin\left(\frac{\sin \hat{\alpha}_{i_q,h}}{\cos \hat{\alpha}_{i_q,v}} \right) \tag{15}$$

EKF-Based Prediction

In order to reduce the overhead of beam sweeping and improve beam alignment accuracy, the CBS predicts the UE's position based on EKF, which linearized the non-linear measurement model to the currently estimated state [14].

The state model at the kth time step is defined as $\mathbf{x_k} = [p_k^x, p_k^y, v_k^x, v_k^y]^T$, where p_k^x, p_k^y are the x-coordinate and the y-coordinate of the vehicle, and v_k^x, v_k^y are the velocity components in the x-direction and the y-direction, respectively. We initialized the state model as $\mathbf{x}_0$ based on beam sweeping and TOA estimation. Furthermore, the state transition model and measurement model are given as

$$\mathbf{x_k} = f(\mathbf{x_{k-1}}) + \mathbf{w_k} \tag{16}$$

$$\mathbf{z_k} = h(\mathbf{x_k}) + \mathbf{v_k} \tag{17}$$

where $\mathbf{z_k}$ is the measurement vector. Moreover, $f(\cdot)$ and $h(\cdot)$ are the state transition and measurement model function respectively. $\mathbf{w_k} \sim N(\mathbf{0}, \mathbf{Q})$ and $\mathbf{v_k} \sim N(\mathbf{0}, \mathbf{R})$ denote process noise vector and measurement noise vector. $\mathbf{Q} \in \mathbb{R}^{2\times 2}$ and $\mathbf{R} \in \mathbb{R}^{2\times 2}$ are the covariance matrices for process noise and measurement noise, respectively.

The assumption that the UE moves straightly with constant velocity results in linear state transition function, which is defined as

$$f(\mathbf{x_{k-1}}) = \mathbf{F}\mathbf{x_{k-1}} = \begin{pmatrix} \mathbf{I_{2\times 2}} & \Delta t\mathbf{I_{2\times 2}} \\ \mathbf{0_{2\times 2}} & \mathbf{I_{2\times 2}} \end{pmatrix} \mathbf{x_{k-1}} \tag{18}$$

where Δt is the time interval between two consecutive states.

Furthermore, the UE's distance and angle is measured by the CBS, which are non-linear with position coordinates. The measurement model function can be expressed as

$$h(\mathbf{x_k}) = \begin{pmatrix} \sqrt{(p_k^x)^2 + (p_k^y)^2} \\ \arctan(p_k^x / p_k^y) \end{pmatrix} \tag{19}$$

The covariance matrix for process noise which is defined based on continuous white noise acceleration model in [15], is given by

$$\mathbf{Q} = \sigma_v^2 \begin{pmatrix} \frac{\Delta t^3}{3}\mathbf{I_{2\times 2}} & \frac{\Delta t^2}{2}\mathbf{I_{2\times 2}} \\ \frac{\Delta t^2}{2}\mathbf{I_{2\times 2}} & \Delta t\mathbf{I_{2\times 2}} \end{pmatrix} \tag{20}$$

where σ_v^2 is the variance of UE's velocity.

In each time step k, the EKF-based estimation method consists of two stages: prediction stage and update stage.

In prediction stage, the priori estimated state vector in current time step $\hat{\mathbf{x}}_{\mathbf{k}|\mathbf{k-1}}$ is obtained based on transition model function given in (18), i.e. $\hat{\mathbf{x}}_{\mathbf{k}|\mathbf{k-1}} = f(\hat{\mathbf{x}}_{\mathbf{k-1}|\mathbf{k-1}})$. Moreover, the priori estimated covariance $\mathbf{P}_{\mathbf{k}|\mathbf{k-1}}$ can be written as

$$\mathbf{P}_{\mathbf{k}|\mathbf{k-1}} = \mathbf{F}\mathbf{P}_{\mathbf{k-1}|\mathbf{k-1}}\mathbf{F}^T + \mathbf{Q} \tag{21}$$

where $\hat{\mathbf{x}}_{\mathbf{k-1}|\mathbf{k-1}}$ and $\mathbf{P}_{\mathbf{k-1}|\mathbf{k-1}}$ are the posterior estimated state vector and covariance at the last time step.

In update stage, the priori estimate which is updated based on measurement model function given in (19), is expressed as

$$\hat{\mathbf{x}}_{\mathbf{k}|\mathbf{k}} = \hat{\mathbf{x}}_{\mathbf{k}|\mathbf{k-1}} + \mathbf{K}_{\mathbf{k}}(\mathbf{z}_{\mathbf{k}} - h(\hat{\mathbf{x}}_{\mathbf{k}|\mathbf{k-1}})) \tag{22}$$

$$\mathbf{P}_{\mathbf{k}|\mathbf{k}} = (\mathbf{I} - \mathbf{K}_{\mathbf{k}}\mathbf{H}_{\mathbf{k}})\mathbf{P}_{\mathbf{k}|\mathbf{k-1}} \tag{23}$$

where $\mathbf{K}_{\mathbf{k}}$ is the Kalman gain given by

$$\mathbf{K}_{\mathbf{k}} = \frac{\mathbf{P}_{\mathbf{k}|\mathbf{k-1}}\mathbf{H}_{\mathbf{k}}^T}{\mathbf{H}_{\mathbf{k}}\mathbf{P}_{\mathbf{k}|\mathbf{k-1}}\mathbf{H}_{\mathbf{k}}^T + \mathbf{R}_{\mathbf{k}}} \tag{24}$$

where $\mathbf{H}_{\mathbf{k}} = \frac{\partial \mathbf{h}}{\partial \mathbf{x}}|\hat{\mathbf{x}}_{\mathbf{k}|\mathbf{k-1}}$ is the Jacobian matrix of the nonlinear measurement model function $h(\cdot)$ evaluated at $\hat{\mathbf{x}}_{\mathbf{k}|\mathbf{k-1}}$, and can be derived as

$$\mathbf{H}_{\mathbf{k}} = \begin{bmatrix} \frac{p_k^x}{\sqrt{(p_k^x)^2 + (p_k^y)^2}}, & \frac{p_k^y}{\sqrt{(p_k^x)^2 + (p_k^y)^2}}, 0, 0 \\ \frac{p_k^y}{(p_k^x)^2 + (p_k^y)^2}, & -\frac{p_k^x}{(p_k^x)^2 + (p_k^y)^2}, 0, 0 \end{bmatrix} \tag{25}$$

3.2 Multi-site Coordination Beam Tracking Scheme

We have mentioned that it is quite difficult to acquire the complete CSI for each site individually, which takes up plenty of pilot resource. The location of multiple BSs and the UE can be used as a link for the CSI nonlinear correlation. Therefore, in this part, we consider to use geometric relationship between locations to determine the optimal beam direction between each TBS and the UE. Subsequently, we proposed a novel scheme for TBS handover based on the UE's position to reduce unnecessary switching on the condition of ensuring good performance.

Serving Beam Inference for TBS

As the UE's position is predicted, instead of exhaustive sweeping on the entire beam set, the serving beam direction between each TBS and the UE can be identified through a beam sweeping within a narrow range around the predicted UE's position. The candidate beam set can be obtained by geometric method based on the AOA between the TBS and the UE. Therefore, the size of candidate beam set significantly decreases, thus leads to low beam training overhead for each TBS.

The estimated azimuth and elevation AOA from each TBS to the UE are given by

$$\tilde{\theta}_{TBS_j} = \arctan\left[\frac{p_{z,TBS_j} - \hat{p}_z}{\sqrt{\left(p_{x,TBS_j} - \hat{p}_x\right)^2 + \left(p_{y,TBS_j} - \hat{p}_y\right)^2}}\right] \tag{26}$$

$$\tilde{\varphi}_{TBS_j} = \arctan\left[\frac{p_{y,TBS_j} - \hat{p}_y}{p_{x,TBS_j} - \hat{p}_x}\right] \tag{27}$$

where $\left(\hat{p}_x, \hat{p}_y, \hat{p}_z\right)$ is the UE's predicted position, and $\left(p_{x,TBS_j}, p_{y,TBS_j}, p_{z,TBS_j}\right)$ is the coordinate of the j-th TBS that known by CBS. Since LoS path has the strongest power, the candidate beam pair for each TBS and UE is obtained around $\tilde{\theta}_{TBS_j}$ and $\tilde{\varphi}_{TBS_j}$. Finally, the best beam pair is selected from the candidate set by beam refinement between each TBS and the UE.

TBS Handover Judgement

Besides serving beam prediction, the CBS will judge whether the serving TBS handover occurs when the UE's position changes. According to RSRP measurement for two adjacent TBSs, the serving TBS with stronger signal can be determined. However, RSRP measurement requires beam training between each TBS and the UE, and the overhead is non-negligible. Note that closer communication distance leads to lower path loss, it is reasonable to choose the serving TBS for the UE based on the distance to each TBS. Although closer TBS may experience deeper fading than the remoter TBS, the distance difference makes the RSRP between two TBSs most likely has a small gap, thus the handover leads to limited gain. Consequently, we propose a joint strategy for TBS handover to reduce the overhead. If the distance difference between UE and two TBSs is larger than a certain threshold, the closer TBS is determined as serving TBS directly. Otherwise, RSRP report about each TBS is used as handover condition, the flow chart is introduced in Fig. 2.

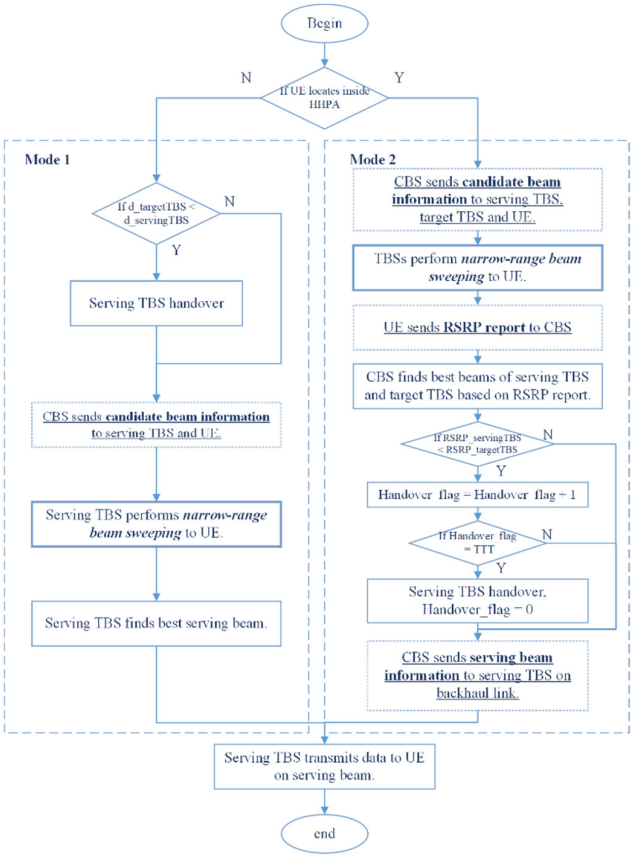

Fig. 2. Flow chart of TBS handover

In the proposed handover method, the serving TBS and target TBS is initialized by CBS before position prediction. We define a high handover probability area (HHPA) whose center at the midpoint of serving TBS and target TBS, and its radius is one-quarter of the distance between two adjacent TBS. The handover condition corresponding to mode 1 and mode 2 depends on whether UE locates inside HHPA, and is introduced as follow.

Mode 1: Firstly, the CBS calculates the distance between each TBS and the estimated UE's position, and chooses the nearest TBS as the serving TBS. Next, the CBS sends control information including candidate beam indexes to the serving TBS and the UE on the backhaul link and PDCCH respectively. Finally, the serving TBS performs beam refinement with the UE on each candidate beam pair and selects the optimal serving beam pair.

Mode 2: The CBS sends candidate beam indexes to each TBS and the UE on the backhaul link and PDCCH respectively. Both the serving TBS and the target TBS

perform beam refinement with UE on candidate beams transmitted by CBS. Subsequently, based on the RSRP report of each beam pair from the UE to the CBS on PUCCH, the CBS finds the best beam pair of the serving TBS and the target TBS with UE. The handover process controlled by the CBS starts when the target TBS becomes stronger than the serving TBS, and is defined as a trigger event. After the trigger event, the CBS waits for a certain time duration i.e. time to trigger (TTT). The TBS handover occurs if the RSRP of the target TBS is always stronger than the serving TBS during TTT, and the serving beam index is transmitted to the serving TBS by the CBS on the backhaul link, whereas the beam index at UE side can be determined by UE itself before RSRP report without feedback from the CBS.

4 Simulation

In this section, we evaluate the performance of the proposed location-based multi-site coordination beam tracking method. In order to make our simulation scenario more realistic, the ray-tracing channel parameters for a practical urban environment is generated by Wireless InSite [16]. As shown in Fig. 3, two TBSs located within the coverage of one CBS are equipped with 8 * 8 UPA, while the CBS is equipped with 16 * 16 UPA. The height of the CBS and TBSs are 32 m and 12 m, respectively, and the downlink (DL) transmit power of TBS is 40 dBm. UE is equipped with 4 * 4 UPA, and moves straightly with constant velocity 20 m/s. The spacing of two adjacent route point is 0.3 m, and the number of route point is set to 500. The quantization resolution in 2D steering codebook is set to 8 and 1 for BS and UE, respectively. With regard to the OFDM configurations, the carrier frequency is 28 GHz, and the bandwidth as well as subcarrier spacing are 100 MHz and 120 kHz, respectively. Furthermore, the noise spectral density is set to −174 dBm/Hz.

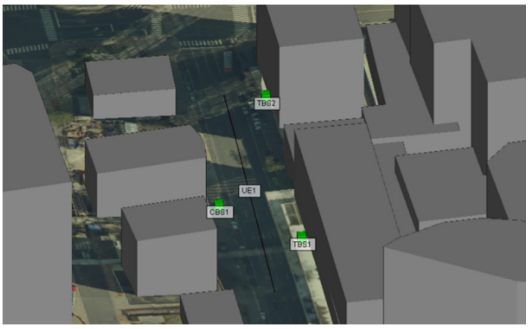

Fig. 3. Simulation scenario

Figure 4 and Fig. 5 show the MSE for estimated distance and AoA against the UL transmit power, respectively. Position is predicted based on UPA in our scheme, while ULA is equipped in [6]. Given that UPA can flexibly adjust beam directions in both

horizon and vertical, it leads to more accurate beam alignment and position prediction than ULA in practical 3D mMIMO scenario. It is shown that the MSE of distance and AoA estimation is reduced significantly by using UPA, which are both at the level of 10^{-3} at high transmit power.

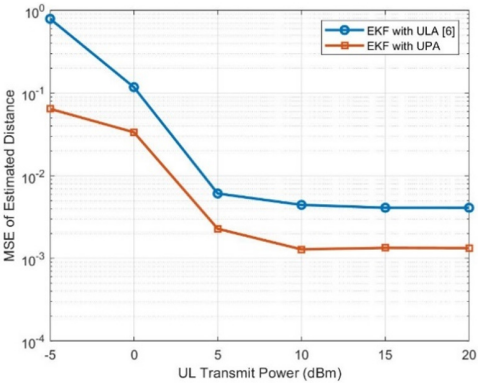

Fig. 4. MSE for distance estimation

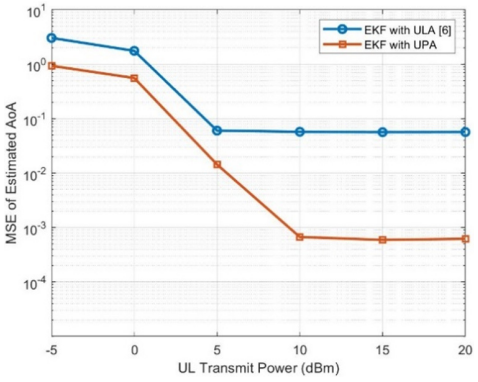

Fig. 5. MSE for AoA estimation

Figure 6 illustrates the average spectral efficiency (SE) in DL from the serving TBS to the UE when the UE moves along the route. The performance of proposed algorithm has 8.8% improvement over the ULA based algorithm in [6] by using the UPA, and achieves about 99% of the upper bound which is defined as the performance with the optimal beamforming vector from UPA codebook by exhaustive beam searching. The result verify that it is reasonable and efficient to track the beam direction for the TBS utilizing the UE's position predicted by the CBS in multi-site scenario, and more accurate position information performs better. In addition, compared with the TBS handover based on RSRP report, the proposed algorithm based on HHPA has almost no performance loss as long as UL transmit power is larger than 10 dBm.

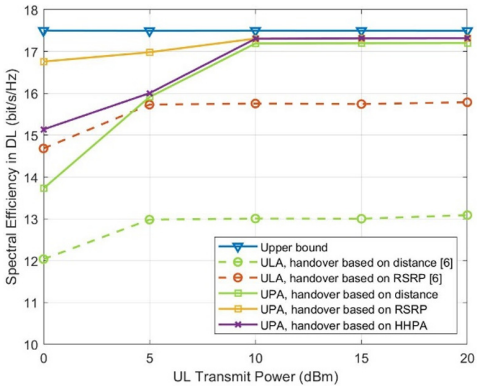

Fig. 6. SE in DL from serving TBS

Figure 7 compares the TBS handover times and beam sweeping complexity for the four schemes. The exhaustive beam searching scheme has the maximum handover times and also the highest beam sweeping complexity which yields unacceptable pilot overhead in each slot. Due to extremely low tracking loss, the complexity of beam training in the proposed multi-site coordination scheme is reduced by about 1000 times because of location-based narrow-range beam sweeping. Furthermore, handover based on HHPA lower the frequent TBS handover, which also promotes the reduction of 1/3 pilot overhead in handover based on RSRP. To sum up, the result shows that the proposed method has a significant advantage in reducing the complexity of beam training and TBS handover times.

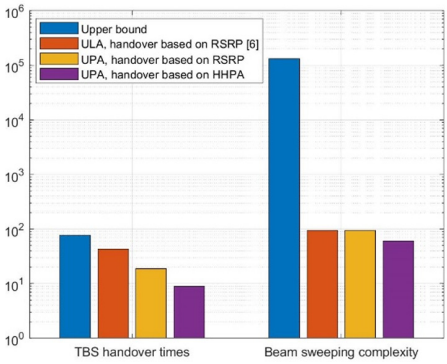

Fig. 7. TBS handover times and beam sweeping complexity, P_t = 15 dBm

5 Conclusion

In this paper, we propose a location-based multi-site coordination beam tracking scheme in HCN for vehicle communications. The entire procedure consists of two stages, i.e. position prediction stage and multi-site coordination stage. In the first stage, according to the accurate spatial position measured by UPA, EKF was applied in the CBS to predict the user's position. In the second stage, the optimal beam pattern at each TBS is inferred based on the geometry approach relied on the UE's position, and the TBS handover is determined by position and RSRP report jointly. The numerical results show that the proposed scheme achieves 99% of the maximum spectral efficiency with low beam sweeping complexity and handover overhead.

Acknowledgement. This work is supported by the National Natural Science Foundation of China under Grant No. 61971069, 61801051, and Key R&D Program Projects in Shanxi Province under Grant No. 2019ZDLGY07-10. This work is also supported by Docomo Beijing Lab.

References

1. Shafi, M., et al.: 5G: a tutorial overview of standards, trials, challenges, deployment, and practice. IEEE J. Sel. Areas Commun. **35**(6), 1201–1221 (2017)
2. Wang, J., et al.: Beam codebook based beamforming protocol for multi-Gbps millimeter-wave WPAN systems. IEEE J. Sel. Areas Commun. **27**(8), 1390–1399 (2009)
3. Va, V., Choi, J., Heath, R.W.: The impact of beamwidth on temporal channel variation in vehicular channels and its implications. IEEE Trans. Veh. Technol. **66**(6), 5014–5029 (2017)
4. Shen, Z., Xu, K., Wang, Y., Xie, W.: Angle-domain channel tracking for high speed railway communications with massive ULA. In: 2018 IEEE 18th International Conference on Communication Technology (ICCT), Chongqing, pp. 159–165 (2018)
5. Zhang, C., Guo, D., Fan, P.: Tracking angles of departure and arrival in a mobile millimeter wave channel. In: 2016 IEEE International Conference on Communications (ICC), Kuala Lumpur, pp. 1–6 (2016)
6. Shaham, S., Kokshoorn, M., Ding, M., Lin, Z., Shirvanimoghaddam, M.: Extended Kalman filter beam tracking for millimeter wave vehicular communications. In: 2020 IEEE International Conference on Communications Workshops (ICC Workshops), Dublin, Ireland, pp. 1–6 (2020)
7. Talvitie, J., et al.: Positioning and location-based beamforming for high speed trains in 5G NR networks. In: 2018 IEEE Globecom Workshops (GC Wkshps), Abu Dhabi, United Arab Emirates, pp. 1–7 (2018)
8. Wang, S., Chen, M., Liu, X., Yin, C., Cui, S., Poor, H.V.: A machine learning approach for task and resource allocation in mobile edge computing based networks. IEEE Internet Things J. (2020). https://doi.org/10.1109/jiot.2020.3011286
9. Zhou, S., Zhao, T., Niu, Z., Zhou, S.: Software-defined hyper-cellular architecture for green and elastic wireless access. IEEE Commun. Mag. **54**(1), 12–19 (2016)
10. Jiang, Z., Chen, S., Molisch, A.F., Vannithamby, R., Zhou, S., Niu, Z.: Exploiting wireless channel state information structures beyond linear correlations: a deep learning approach. IEEE Commun. Mag. **57**(3), 28–34 (2019)

11. Chen, S., et al.: Remote channel inference for beamforming in ultra-dense hyper-cellular network. In: GLOBECOM 2017 – 2017 IEEE Global Communications Conference, Singapore, pp. 1–6 (2017)
12. Chen, S., Jiang, Z., Zhou, S., Niu, Z.: Time-sequence channel inference for beam alignment in vehicular networks. In: 2018 IEEE Global Conference on Signal and Information Processing (GlobalSIP), Anaheim, CA, USA, pp. 1199–1203 (2018)
13. Goldsmith, A.: Wireless Communications. Cambridge University Press, Cambridge (2005). https://doi.org/10.1017/CBO9780511841224
14. Talvitie, J., Levanen, T., Koivisto, M., Valkama, M.: Positioning and tracking of high-speed trains with non-linear state model for 5G and beyond systems. In: 2019 16th International Symposium on Wireless Communication Systems (ISWCS), Oulu, Finland, pp. 309–314 (2019)
15. Bar-Shalom, T.K.Y., Li, X.R.: Estimation with Applications to Tracking and Navigation: Theory. Algorithms and Software. Wiley, Hoboken (2002)
16. Remcom, Wireless insite. http://www.remcom.com/wireless-insite